Hindawi
Scientific Programming
Volume 2023, Article ID 9864697, 1 page
https://doi.org/10.1155/2023/9864697

Retraction

Retracted: Intelligent Evaluation Method of Pressure Relief Gas Drainage in Goaf Based on IoT Perception

Scientific Programming

Received 1 August 2023; Accepted 1 August 2023; Published 2 August 2023

This article has been retracted by Hindawi following an investigation undertaken by the publisher [1]. This investigation has uncovered evidence of one or more of the following indicators of systematic manipulation of the publication process:

(1) Discrepancies in scope
(2) Discrepancies in the description of the research reported
(3) Discrepancies between the availability of data and the research described
(4) Inappropriate citations
(5) Incoherent, meaningless and/or irrelevant content included in the article
(6) Peer-review manipulation

The presence of these indicators undermines our confidence in the integrity of the article's content and we cannot, therefore, vouch for its reliability. Please note that this notice is intended solely to alert readers that the content of this article is unreliable. We have not investigated whether authors were aware of or involved in the systematic manipulation of the publication process.

Wiley and Hindawi regrets that the usual quality checks did not identify these issues before publication and have since put additional measures in place to safeguard research integrity.

We wish to credit our own Research Integrity and Research Publishing teams and anonymous and named external researchers and research integrity experts for contributing to this investigation.

The corresponding author, as the representative of all authors, has been given the opportunity to register their agreement or disagreement to this retraction. We have kept a record of any response received.

References

[1] W. Cao, "Intelligent Evaluation Method of Pressure Relief Gas Drainage in Goaf Based on IoT Perception," *Scientific Programming*, vol. 2022, Article ID 7594388, 12 pages, 2022.

Hindawi
Scientific Programming
Volume 2022, Article ID 7594388, 12 pages
https://doi.org/10.1155/2022/7594388

Research Article

Intelligent Evaluation Method of Pressure Relief Gas Drainage in Goaf Based on IoT Perception

Wentao Cao

Department of Intelligent Manufacturing and Intelligent Mining, Yuncheng Vocational and Technical University, Yuncheng 044000, Shanxi, China

Correspondence should be addressed to Wentao Cao; 1017010310@st.usst.edu.cn

Received 29 July 2022; Revised 31 August 2022; Accepted 10 September 2022; Published 19 September 2022

Academic Editor: M. A. Rashid Sarkar

The pressure relief gas drainage in goaf is the main control method of mine gas. This paper has been designed to study how to analyze and study the gas drainage of goaf pressure relief based on the perception layer of the Internet of Things. The intelligent evaluation of pressure relief gas drainage in goaf is described. This paper has raised the problem of gas extraction, which is based on the Internet of Things, so it has elaborated on the data-level fusion-related algorithms for sensing coal mine safety, and the case design and analysis of the prediction model and intelligent evaluation have been carried out. Aiming at the problem of intelligent grading of gas drainage evaluation in goaf, data preprocessing is performed on the drainage metering data. Using a deep learning evaluation method based on a convolutional neural network (CNN), an intelligent evaluation model is constructed for gas extraction. Compared with the classification model of the shallow neural network, the CNN classification model is more suitable for gas intelligence evaluation and has higher accuracy due to the good learning ability and accuracy of the deep neural network. When the learning rate is 0.1 and the batch is 256, the prediction effect of the CNN pressure relief gas intelligent classification model is the best, which can effectively provide classification results.

1. Introduction

In the normal production process of coal mines, a large amount of gas would flow to the working face, most of which are gas gushing from the goaf. The gas in the goaf is generated by the discharge of adjacent layers, unmined layers, and coal left over from the working face into the gob. Gas disaster is the most important form of disaster that affects the safe and efficient mining of mines, which often causes major economic losses and a large number of casualties in mines. In many areas, the mining working face adopts the method of layered mining, and the pressure relief of the bottom coal in the goaf would produce a large amount of gas, which brings new challenges to gas disaster management. As coal mining depth increases, so does the coal seam gas content and gas gushing volume. Gob gas is one of the main sources of gas gushing from the working face, accounting for about 40–60%. The proportion is higher in mines with carbon deposits. The wide application of efficient working face production and coal cavitation technology has brought economic benefits to coal enterprises and enterprises. At the same time, it would increase gas emission intensity and emissions, which would be a long-term problem threatening the safety of coal mine production.

Through data collection, modeling, and training methods, this paper has proposed the gob pressure relief gas drainage evaluation index body and has constructed the gob pressure relief gas drainage evaluation index body based on a long short-term memory network (LSTM). The exponential prediction model has formed an intelligent assessment method for gas drainage, and a gas drainage assessment system has been developed. The innovation of this paper is that through the enrichment of the IoT perception layer and data fusion, the optimal design of the gas extraction model in the goaf is studied, and intelligent evaluation is carried out. The research in this paper plays an important role in gas extraction in the coal mine.

2. Related Work

At present, great progress has been made in the research on gas drainage in the same goaf, and it has also been widely used in practice. Zhang et al. established a two-medium coupled model in order to study the multiphase multifield coupling problem of gas drainage, which has described the gas-air mixture flow by considering the influence of matrix shrinkage and effective stress on coal permeability [1]. Evanoski-Cole et al. measured winter aerosols and aerosol precursors in national parks and found regional elevated PM2.5 concentrations in the Bakken region [2]. Goodman et al. investigated the physical and substantial changes of the carbonate-rich Utica Shale after CO_2 openness when a slight film of water exists on the shale surface [3]. Zhao et al. endeavored to fill this hole by fostering a monetary improvement model for oil and gas extraction to examine the effect of maker sponsorship expulsion [4]. Utilizing a devoted overview of 4992 respondents, Andersson-Hudson et al. explored the design of UK public mentalities towards shale gas extraction. It has been found that public mentalities towards shale gas extraction have a one-layered structure, so that all inquiries concerning the benefits and constraints of extraction are viewed as an issue. The results have suggested that information has an important role in regulating responses to shale gas. This factor has implications for how governments approach policies related to shale gas extraction [5]. However, they did not study the intelligent evaluation model of pressure relief gas drainage in goaf nor did they study the effect of intelligent evaluation.

The Internet of Things (IoT) is a unique worldwide organization of data that is turning into an indispensable piece of the Internet representing things to come. It is composed of Internet-connected objects such as RFID, sensors, actuators, and other instruments and smart devices. Perera et al. reviewed north of 100 IoT brilliant arrangements available and painstakingly concentrated on them to decide the innovations, capabilities, and applications utilized [6]. Stojkoska and Trivodaliev defined the main characteristics of the overall framework of smart homes from the literature review, a general description of the smart home management model based on the overall framework [7]. Ni et al. examined the design and quality of the haze registry and focused on key parts of the haze hub, including ongoing management, transient capacity, information dissemination, and decentralized processing. Given the various jobs at the smog center, it is also considering using mist to help with IoT applications [8]. Li et al. introduced deep learning for IoT into the edge computing environment, designing a novel offloading strategy to optimize the performance of IoT deep learning applications through edge computing [9]. Siow et al. reviewed these works in terms of the utility of IoT and big data analytics in creating efficient, effective, and innovative applications and services for a wide range of domains. They looked at some of the trade-offs in IoT analytics that may affect future research [10]. However, they have not yet applied the Internet of Things to the research on the intelligent evaluation model of pressure relief gas drainage in goaves.

3. Information Processing Method Based on IoT Perception

3.1. Internet of Things

3.1.1. Overview. The Internet of Things (IoT) is the product of the continuous development of the Internet, ubiquitous computer technology, and wireless communication technology and refers to ubiquitous equipment and information detection technologies, such as RFID technology, GPS technology, and smartphones. For any objects and processes that need to be connected, monitored, and operated, various data information, such as sound, heat, quantity, chemical biology, and location information, are collected, combining the vast Internet to form a ubiquitous network with wider coverage [11]. The ultimate goal of IoT is to establish extensive connections between things, things and people, and people to facilitate communication, identification, management, and control of information. The conceptual model of IoT is shown in Figure 1.

Compared with the traditional Internet, IoT has its distinctive characteristics: it is a ubiquitous network built on the Internet, and it is a wide-ranging application of various technological concepts. IoT not only provides sensor connectivity but also has intelligent processing capabilities in itself.

3.1.2. Technical Framework. From the current research status, the three-layer architecture of the Internet of Things has been widely recognized and divided into three parts [12]. The technical architecture is shown in Figure 2.

The IoT awareness layer is at the bottom of the IoT architecture. It consists of various sensors, a control unit, a network communication unit, and a smart door that accesses the sensors, collects data, and links the perception layer with the network layer [13, 14]. Compared with the traditional Internet, IoT has its distinctive characteristics: it is a ubiquitous network built on the Internet, and it is a wide-ranging application of various technological concepts. IoT not only provides sensor connectivity but also has intelligent processing capabilities in itself.

The network layer includes the Internet, personal area network, mobile communication network, network transmission system, and a business platform for integrating and opening data resources, providing services such as open networks and integration and opening of data resources. In terms of network access, the network technologies used include ADSL, LAN, GPRS, 3G, LTE, and Wi-Fi. The resource integration platform should provide convenient interfaces for data input and data integration and output. Therefore, a REST architecture can be adopted to remove data from resources and provide users with a unified HTTP-based interface method.

The application layer is the user-facing "interface" of IoT. In combination with specific industry needs, IoT applications are created for various industries based on the perception layer and network layer, such as environmental monitoring, natural disaster warning, smart home and

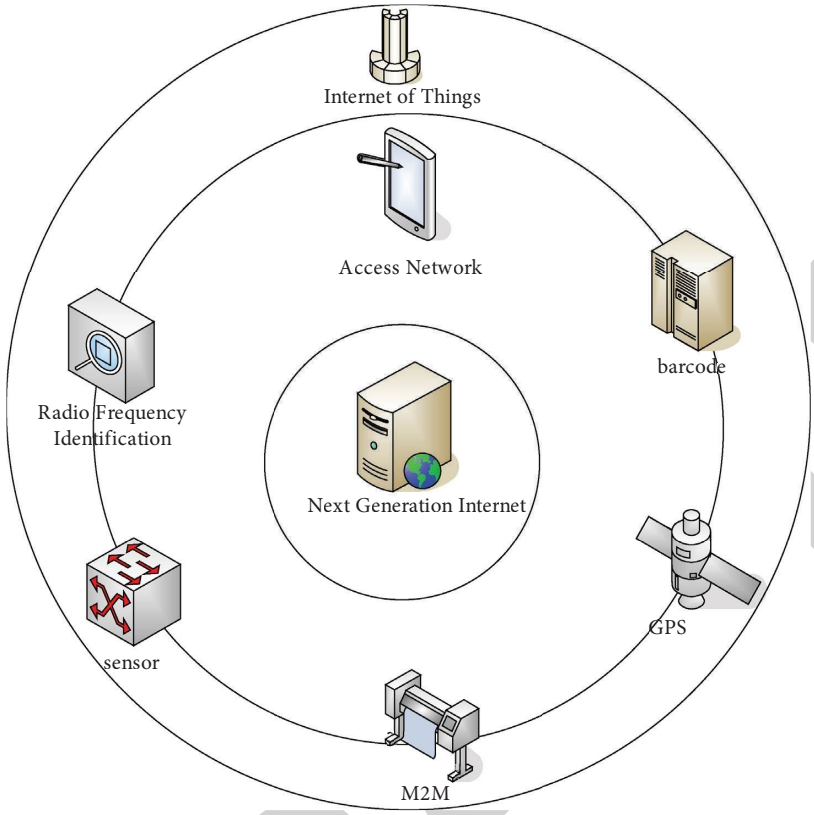

Figure 1: IoT conceptual model.

intelligent transportation, remote medical monitoring and health monitoring, and remote production monitoring. The intelligence and practicability of IoT are understood, so that IoT can ultimately serve people's production and life and serve the progress of social productivity.

3.2. Perception Layer

3.2.1. Diversity of Perception Layer Sensors. From the current state of research and production, the diversity and heterogeneity of sensor interfaces are still unavoidable issues in IoT R&D. While the International Organization for Standardization has defined software and hardware models for networked smart sensors and electronic TEDS data sheets, as well as detailed requirements for data transmission, addressing, deactivation, and activation of smart sensors, they have not yet been adopted on a large scale.

According to different working principles, sensors can usually be divided into two categories, as shown in Figure 3(a); according to different types of measurement data, sensors can be divided, as shown in Figure 3(b); according to the different types of output signals, sensors can be divided into three categories as shown in Figure 3(c).

3.2.2. Wireless Sensor

(1) Node Composition. The sensor node consists of four parts, namely, energy supply module, sensor module, wireless communication module, and processor module, as shown in Figure 4 [15]. The sensor module completes the data collection and conversion of the monitoring area. The processor module is responsible for managing the operation of the entire node. The sensor stores and processes the data collected by itself and the data sent from other countries. The wireless communication unit is a wireless communication node with other devices, sending and receiving collected data and exchanging control messages. The energy supply module provides the energy required for the operation of the sensor node, usually using tiny batteries.

(2) Basic Structure. Network topology is an important network management model, which can provide many network characteristics, such as the number, distribution, and network connectivity of active nodes. Wireless sensor networks are a kind of self-organizing network. The formation and operation of the network are largely carried out autonomously by many network nodes and do not require manual configuration. Therefore, in the initial stages of network creation, an autonomous generation mechanism of a specific topology should be employed. The basic topological structures of wireless sensor networks can be divided into three types: chain-based linear structures, web-based planar structures, and cluster-based hierarchical stereo structures [16, 17].

(a) Chain-based linear structure: Figure 5 shows the chain-based linear network structure. Several nodes form a chain, and each data source reaches the sink

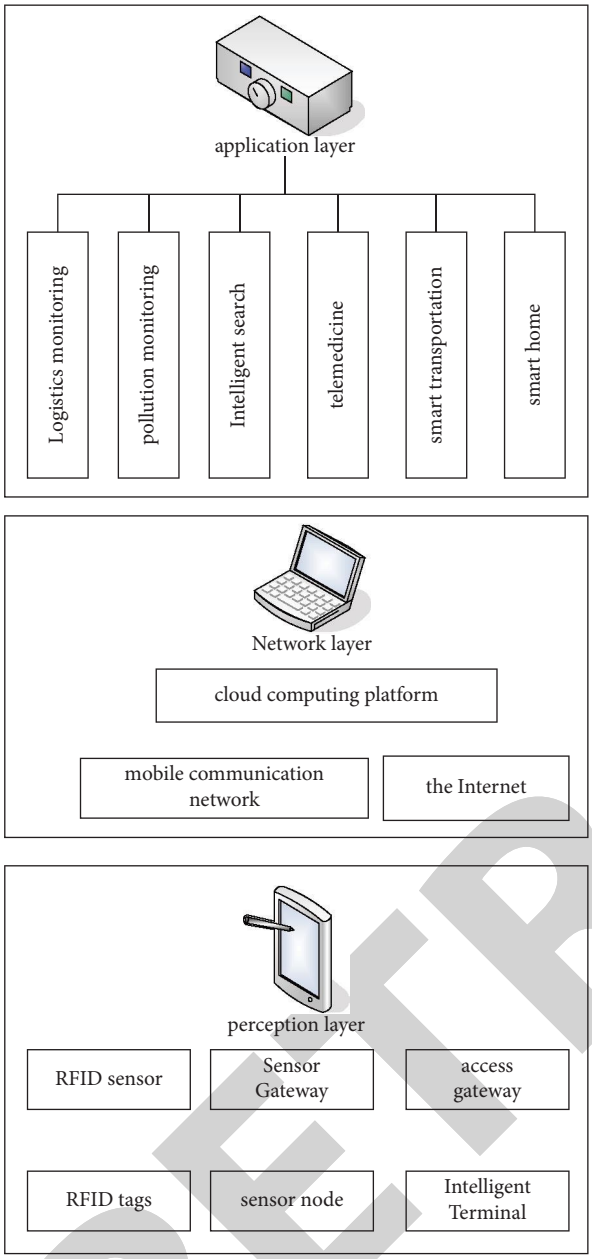

Figure 2: IoT three-tier application architecture.

node along its own data chain. In the chain formation process, the shortest path should be considered to avoid energy waste. In this way, the network routing protocol is relatively simple, and the robustness of the network is poor. The failure of a node affects the information transfer of this connection [18].

(b) Web-based flat structure: the web-based flat structure corresponds to wireless sensor networks using transmit, flood, and multitransmit routing mechanisms, as shown in Figure 6. Such network information is transmitted through multiple routes, which improve the reliability of communication; the network is robust and has good connectivity, and single node failure and communication connection failure would not cause network separation. However, the huge disadvantage of this network topology is the low energy efficiency [19, 20].

(c) Cluster structure: in the data processing process based on the hierarchical structure of the cluster, each member of the cluster transmits the data to the cluster head, where the data merging process is completed and then transmits it to the user node through multiple transformations of other nodes. In a mine, the working face is long and narrow with a relatively small width, so the cluster structure is more advantageous, as shown in Figure 7. Communication within each cluster can be single-hop or multihop communication. Once the information reaches the cluster head, the information would be passed to the upper layer network. Advanced networks would use higher transmission bandwidth or connect advanced networks to wired networks.

From the analysis of the above topology, nodes in a wireless sensor network usually communicate in three ways: direct transmission (each node sends information directly to the base station), multihop mode (data transmission is sent to the base station through each node), and cluster-based mode.

3.3. Data-Level Fusion of Coal Mine Safety Perception. When multiple sensors measure the same index, set the probability distribution of the data measured by sensor a and sensor b to $g_a(x)$ and $g_b(x)$; then, the conditional probability function is as follows:

$$g_{ab} = g_a\left(x_b \mid x_a\right). \tag{1}$$

Then, the confidence distance measurement d_{ab} of two sensors measuring the same index parameter is as follows:

$$\begin{aligned} d_{ab} &= d_{ba} \\ &= \left|\int_a^b g_a\left(x \mid x_a\right) g_a\left(x_a\right) dx\right| + \left|\int_b^a g_b\left(x \mid x_b\right) g_b\left(x_b\right) dx\right|. \end{aligned} \tag{2}$$

In the equation, $|\int_a^b g_a(x \mid x_a) g_a(x_a) dx|$ and $|\int_b^a g_b(x \mid x_b) g_b(x_b) dx|$ are the area covered by the probability distribution, between the measurements of sensors x_a and x_b, respectively, $0 \le d_{ab} \le 1$. Specifically, when $d_{ab} = 0$, it means that x_a and x_b are exactly equal, when $d_{ab} = -1$, it means that x_a and x_b are quite different.

Then, the complete steps of the dynamic clipping filtering algorithm are as follows.

A confidence distance measure may represent a probabilistic distance, which reflects the degree of agreement between the measurements of two sensors. The higher the d_{ab} value, the greater the probability of the sensor's measurement error. The lower the d_{ab} value, the more the measurement values of the two sensors can reflect the "true value" of the measured object. Then, the complete steps of the dynamic clipping filtering algorithm are as follows.

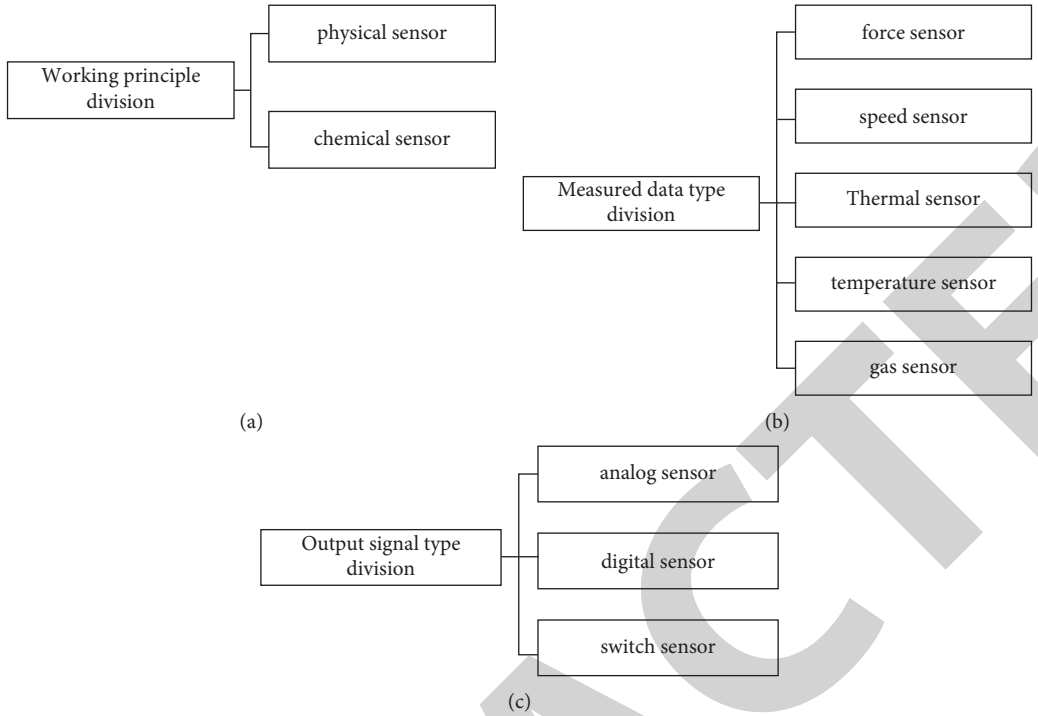

Figure 3: Classification of sensors: (a) divided by working principle, (b) by type of data measured, and (c) by output signal type.

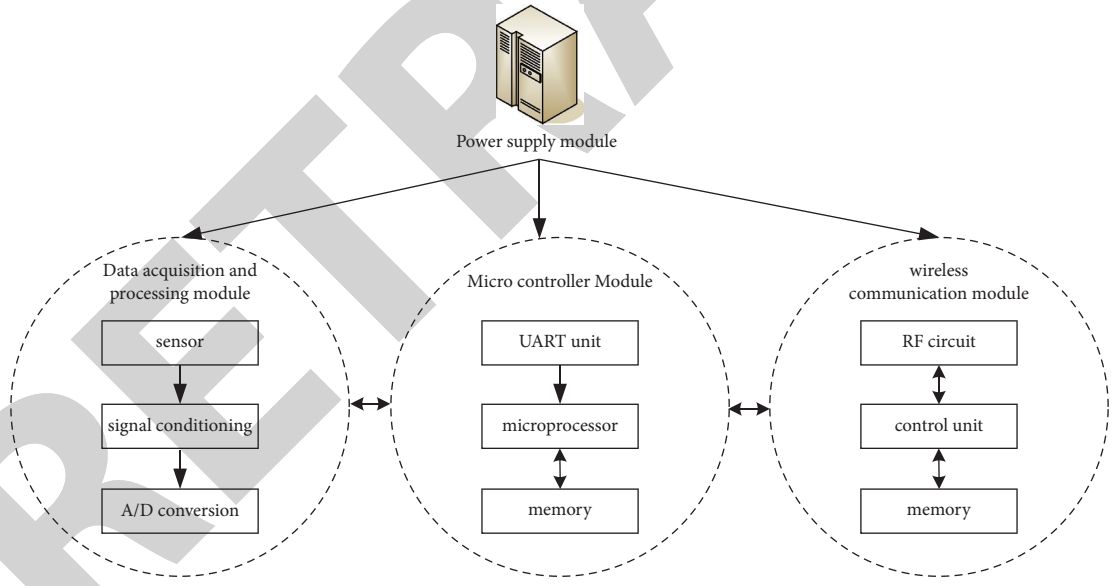

Figure 4: Sensor node architecture.

The measurement series is obtained by taking samples in a time series over a specified time period: $X_1, X_2, ..., X_m$.

Calculate the increments Y_a, $Y_1 = X_2 - X_1, Y_2 = X_3 - X_2, \ldots, Y_a = X_{a+1} - X_a, \ldots, Y_{m-1} = X_m - X_{m-1}$ of adjacent measurements.

$\triangle$ is the maximum allowable increase of two adjacent measured values, and its value can be determined according to the average change rate V_{age} of X_a and the sampling period Z, namely,

$$\Delta = ld_{ab}V_{\text{age}}Z. \tag{3}$$

Calculation of $\triangle$ is the key to the algorithm, which requires an accurate estimate of the range of V_{age}. l is the filter coefficient, the size of which is adjustable and depends on the processing accuracy of the system.

If $|Y_a| > \Delta$, it means that adjacent values have an increasing range larger than $\triangle$. Then, it is necessary to compare their timestamps D_{ZW_a} and recalculate the area Δ' limited by the growth range:

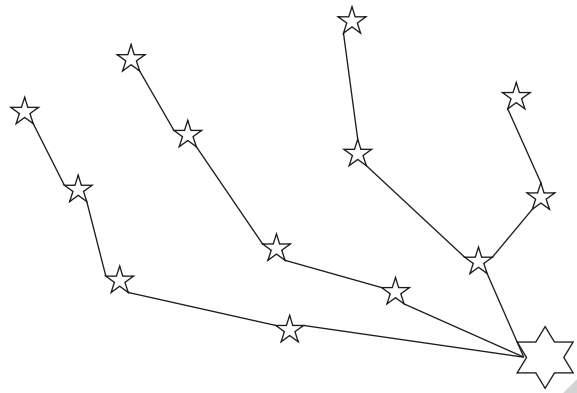

Figure 5: Chain-based linear structure.

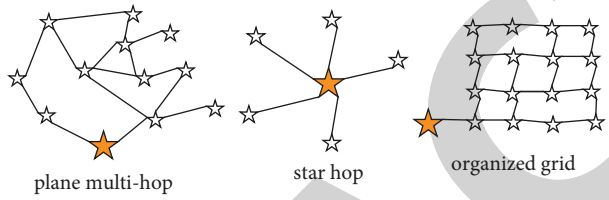

Figure 6: Web-based flat structure.

Figure 7: Two-layer cluster structure.

$$\Delta' = \Delta \frac{\left| D_{ZW_{a+1}} - D_{ZW_a} \right|}{Z}. \tag{4}$$

If $|Y_a| > \Delta'$, continue to calculate $|Y_{a+1}|$. If $|Y_{a+1}| > \Delta$, judge X_a as a negligence error point. If $|Y_{a+1}| > \Delta$ and $|Y_{a+1}| > \Delta'$, it can be judged that X_{a+1} is a negligence error point. If $|Y_{a+1}| < \Delta'$, it can be judged that X_a is a negligence error point.

Let the variance of m sensors be $\delta_1^2, \delta_2^2, \ldots, \delta_m^2$, and the actual value to be estimated is x. The measurement data of the a-th sensor is x_a. They are all unbiased estimates. The fusion weighting factor corresponding to each sensor is v_a. The sampling time of the sensor is l. Then, the actual value $\hat{x}$ and weighting factor obtained after fusion satisfy the following equation:

$$\begin{cases} \widehat{x} = \sum_{a=1}^{m} v_a x_a \\ \sum_{a=1}^{m} v_a = 1 \end{cases}. \tag{5}$$

The total mean squared error is as follows:

$$\begin{aligned} \delta^2 &= E\left[(x-\widehat{x})^2 \right], \\ &= E\left[\sum_{a=1}^{m} v_a^2 (x-x_a)^2 + 2 \sum_{a=1,b=1,a\neq b}^{m} v_a v_b (x-x_a)(x-x_b) \right]. \end{aligned} \tag{6}$$

Since they are independent of each other and are unbiased estimates of x, it can be obtained as follows:

$$\begin{aligned} E\left[(x-x_a)(x-x_b)\right] = 0, \\ (a \neq b, a = 1, 2, \ldots, m; b = 1, 2, \ldots, m). \end{aligned} \tag{7}$$

Therefore, δ^2 can be written as follows:

$$\delta^2 = E\left[\sum_{a=1}^{m} v_a^2 (x-x_a)^2 \right] = \sum_{a=1}^{m} v_a^2 \delta_a^2. \tag{8}$$

It can be seen from equation (8) that the total mean square error δ^2 is a square multivariate function of each weighting factor, so δ^2 must have a minimum value.

The calculation of the minimum value is the weighting factor $v_1, v_2, \ldots, v_a$, that is, the end of the function that satisfies the constraints of equation (5).

According to the theory of finding the extreme value of the multivariate function, the extreme value of formula (9) is found by using the Lagrangian method:

$$f(v, \delta) = \sum_{a=1}^{m} v_a^2 \delta_a^2 + \varepsilon \left(\sum_{a=1}^{m} v_a^2 - 1 \right). \tag{9}$$

The weighting factor corresponding to the minimum total mean squared error can be as follows:

$$v_a^* = \frac{1}{\delta_1^2 \sum_{a=1}^{m} 1/\delta_1^2}. \tag{10}$$

The corresponding minimum mean square error is as follows:

$$\overline{\delta}^2_{\min} = \frac{1}{l \sum_{a=1}^{m} 1/\delta_1^2}. \tag{11}$$

As can be seen from the above analysis, the variance δ_a^2 of each sensor determines the optimal weighting factor v_a^*. δ_a^2 is usually unknown. However, according to the corresponding algorithm, they are determined from the measurements provided by a single sensor. Then, the method to calculate the sensor variance δ_a^2 is discussed.

There are two different sensors i and j, whose measurement values are x_i and x_j, respectively. The corresponding observation errors are ψ_i and ψ_j, respectively; then, there are

$$\begin{cases} \psi_i = x - x_i \\ \psi_j = x - x_j \end{cases}. \tag{12}$$

In the equation, the zero-mean stationary noise is expressed as ψ_i, ψ_j, and the variance of sensor i is

$$\delta_i^2 = E\left(\psi_i^2\right). \tag{13}$$

Because ψ_i and ψ_j are not correlated with each other and the mean value is zero and x is not correlated, the cross-correlation function I_{ij} of x_i and x_j satisfies

$$I_{ij} = E\left(x_i x_j\right) = E\left(x^2\right). \tag{14}$$

The autocorrelation function I_{ii} of x_i satisfies

$$I_{ii} = E\left(x_i x_i\right) = E\left(x^2\right) + E\left(\psi_i^2\right). \tag{15}$$

Subtract equation (14) from equation (15) to get

$$\delta_i^2 = E\left(\psi_i^2\right) = I_{ii} - I_{ij.} \tag{16}$$

For its I_{ii}, I_{ij} calculation, in the above equation, it can be obtained by calculating its expected value in the time domain.

Let the expected value of the time domain estimate of I_{ii} be $I_{ii}(l)$, then it can be obtained as follows:

$$\begin{aligned} I_{ii} &= \frac{1}{l} \sum_{a=1}^{l} x_i(a) x_j(a) = \frac{1}{l} \left[\sum_{a=1}^{l} x_i(a) x_i(a) + x_i(l) x_i(l) \right], \\ &= \frac{l-1}{l} I_{ii}(l-1) + \frac{1}{l} x_i(l) x_i(l). \end{aligned} \tag{17}$$

Similarly,

$$I_{ii} = \frac{l-1}{l} I_{ij}(l-1) + \frac{1}{l} x_i(l) x_j(l). \tag{18}$$

Then, the sensor $j\,(j \neq i; j = 1, 2, \ldots, m)$ and sensor i are correlated to obtain the value of $I_{ij}(l)\,(j \neq i; j = 1, 2, \ldots, m)$. Therefore, for I_{ij}, the mean value $\overline{I}_i(l)$ of $I_{ij}(l)$ can be further used as its estimate, that is,

$$I_{ij} = \overline{I}_i(l) = \frac{1}{m-1} \sum_{j=1, j\neq i}^{m} I_{ij}(l). \tag{19}$$

Thereby, the autocorrelation function and the I_{ii} and I_{ij} cross-correlation functions are obtained from the measured value of each sensor and the estimated value in the time domain, so that the variance δ_a^2 of each sensor can be estimated.

4. Intelligent Evaluation Experiment and Pressure Relief Gas Extraction in Goaf

4.1. Experimental Dataset. The experimental dataset is collected by collecting gas extraction data from coal mines. The dataset records 10,000 pieces of gas timing information. It includes the data of time, drainage concentration, mixed flow, accumulated daily drainage flow, scalar, gas

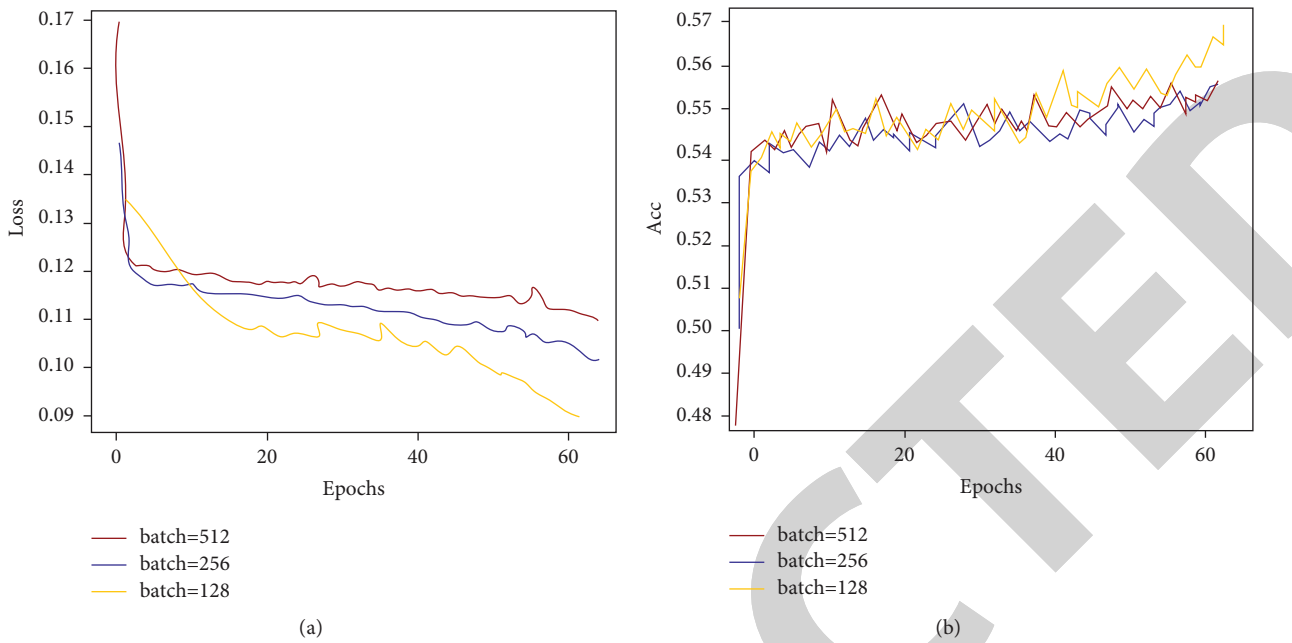

Figure 8: Change images of loss and acc under different batch values. (a) Loss value. (b) Accuracy.

concentration in the upper corner, gas concentration in return airflow, working face gas concentration, working face air volume, temperature, and drainage negative pressure.

The loss function is used to evaluate the model for training and testing of the coal mine gas dataset separately.

4.2. Prediction Model Step Size Tuning. The time step (batch size) represents the sequence length that the LSTM can use. It reflects the data association length. When the amount of data is large, the batch size can be appropriately reduced. Due to the large amount of data, the memory is insufficient, but excessive reduction will cause the model to fail to converge. The choice of batch size first determines the direction of iterative descent. When the dataset is small, the complete data form can be used. Therefore, the orientation of the full dataset is a better representation of the sample population. An appropriate global learning rate is chosen when the binning values for the different weights are very different. A modest increase in batch size can improve memory usage and operational efficiency and require fewer repetitions for a run. The direction of convergence is more accurate and the oscillation is smaller. The blind increase of batch size would lead to the decline of model prediction accuracy, resulting in problems such as difficulty in convergence. Therefore, the selection of the appropriate batch size has a key impact on the prediction accuracy and operating efficiency of the model.

In order to study the effect of batch size on the model, as shown in Figure 8(a), in this experiment, based on the principle of "broad" strategy, the batch size is gradually increased, and the performances of batch sizes of 128, 256, and 512 are compared, respectively. As shown in Figure 8(b), using the established LSTM model, the number of training epochs is set to 64. The batch sizes are 512, 256, and 128, and the loss function is MSE. The training loss and accuracy are shown in Figure 8.

Table 1: Comparison of LSTM loss values for training with different batches.

Batch	512	256	128
Loss (epoch = 1)	0.167	0.151	0.129
Loss (epoch = 24)	0.118	0.120	0.118
Loss (epoch = 48)	0.115	0.114	0.110
Loss (epoch = 64)	0.113	0.105	0.098

Table 2: Comparison of LSTM loss values acc for training with different batches.

Batch	512 (%)	256 (%)	128 (%)
Loss (epoch = 1)	49.95	50.20	50.76
Loss (epoch = 24)	52.34	54.12	53.82
Loss (epoch = 48)	54.02	54.99	55.40
Loss (epoch = 64)	55.48	55.71	56.95

As shown in Figure 8, with the increase of the batch, although the training error of the model is decreasing, the convergence speed of the loss is gradually slowing down, and the training accuracy is also decreasing. The above results verify the loss value (loss) and accuracy (acc) of different loss function models, and the results are shown in Tables 1 and 2. When the batch is 128, the loss of the model decreases the fastest and is always smaller than the loss value of other batch training, and the final training accuracy of the model is the highest. When the batch is 512, the model converges faster during the first 24 epochs. At the same time, the larger the batch, the larger the initial loss value. The faster the convergence, the lower the accuracy. The smaller the batch, the smaller the initial loss value. The accuracy is higher, but the

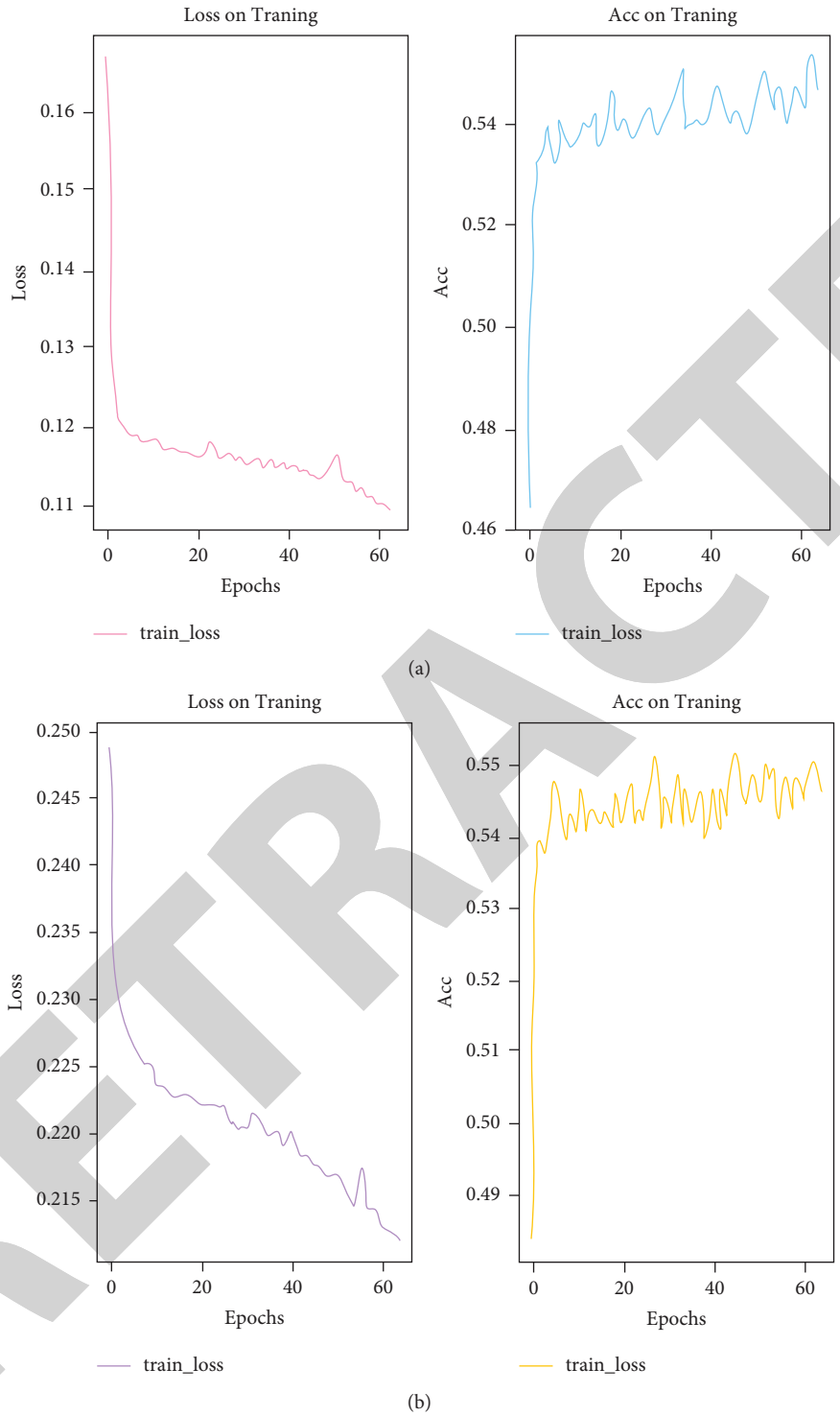

Figure 9: Loss and acc change images under different loss functions. (a) Loss and acc change images when the loss function is MSE. (b) Loss and acc change images when the loss function is MAE.

convergence speed is stable. However, when training, the smaller the batch size, the longer the training time.

4.3. Prediction Model Loss Function Tuning. The loss function is a function that expresses how far the model predicted value deviates from the actual value. The lower the value of the loss function, the closer it is to 0. It indicates that the knowledge learned by the model is more accurate. The more accurately it can represent the actual value, the better the performance of the model. The loss value and accuracy of training are shown in Figure 9.

Using the established LSTM model, the number of training epochs is set to 64. The batch size is 512, and the loss

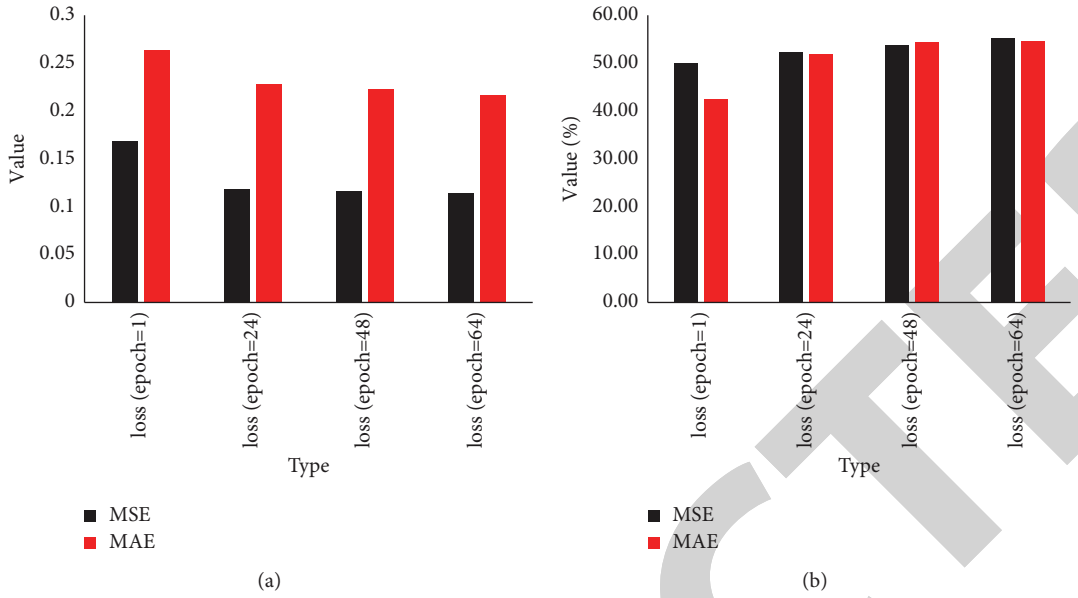

Figure 10: Comparison of LSTM loss values loss and acc for different loss functions. (a) Comparison of LSTM loss values for different loss functions. (b) Comparison of LSTM loss values acc for different loss functions.

Table 3: CNN-based intelligent evaluation model training classification results.

Parameter		Classification				
Batch	Lr	Class I	Class II	Class III	Class IV	Class V
128	0.001	1	0.90	0.97	0.88	0.52
128	0.01	1	0.90	0.97	0.88	0.52
128	0.1	1	1	1	0.88	0.52
256	0.001	1	0.90	0.97	0.88	0.52
256	0.01	1	1	1	0.95	0.52
256	0.1	1	1	1	0.88	0.52
512	0.001	1	0.90	0.97	0.88	0.52
512	0.01	1	1	1	0.88	0.52

function is MSE. The training loss and accuracy are shown in Figure 9(a).

Using the established LSTM model, the number of training rounds epochs is set to 64. The batch size is 512, and the loss function is MAE. The training loss and accuracy are shown in Figure 9(b).

The above results verify the loss value (loss) (Figure 10(a)) and accuracy (acc) (Figure 10(b)) of different loss function models. The results are shown in Figure 10. When the loss function is MSE, the loss of the model decreases the fastest and is always smaller than the loss value of other loss functions. The final training accuracy of the model is the highest. When the loss function is MAE, the model converges faster during the first 24 epochs. After that, the loss of the model does not change significantly, and the model converges to a local optimum. After training, the accuracy of the model is not much different from the accuracy of other loss functions. In order to make the training time cost smaller and the convergence faster, this paper chooses MSE as the loss function.

4.4. Intelligent Evaluation Results. Based on the intelligent evaluation system of pressure relief gas extraction, combined with the gas extraction measurement data of a coal mine, there are a total of 10,000 pieces of data. In this experiment, the CNN model is used for intelligent evaluation of pressure relief gas extraction.

Table 3 shows that the CNN pressure relief gas intelligent evaluation model has the best classification accuracy when the learning grate is 0.1 and the batch is 256. The accuracy of type I evaluation results is 1, the accuracy of type II evaluation results is 1, the accuracy of type III evaluation results is 1, the accuracy of type IV evaluation results is 0.95, and the accuracy of type V evaluation results is 0.52.

In order to verify the reliability and applicability of the CNN extraction intelligent evaluation model proposed in this paper, in addition, this experiment is based on the trained CNN extraction intelligent evaluation model, and the measurement data are extracted from July 10th to July 16th in a certain place. The detailed data are shown in Table 4.

The classification results using the CNN extraction intelligent evaluation model are shown in Table 5.

In the classification results of the sampling measurement data of this place using the CNN intelligent evaluation model for rice extraction, the sampling results of the place on the

Table 4: Drainage metering data.

Data	7.10	7.11	7.12	7.13	7.14	7.15	7.16
Working face air volume (m^3)	1230	1230	1230	1230	1230	1230	1230
Upper corner gas concentration (%)	0.40	0.38	0.44	0.48	0.36	0.36	0.40
Return airflow gas concentration (%)	0.32	0.30	0.28	0.28	0.30	0.30	0.30
Working face gas concentration (%)	0.18	0.18	0.26	0.30	0.20	0.25	0.26
Drainage temperature (°C)	22.00	22.00	18.00	21.00	19.00	22.00	22.00
Drainage mixed flow (m^3/d)	25.02	24.11	26.28	22.99	22.42	21.93	22.11
Drilling concentration (%)	22.00	13.80	19.50	9.40	8.20	7.10	6.80
Drainage pure flow (m^3/d)	5.40	3.20	4.98	2.04	1.63	1.43	1.57
Drainage negative pressure (kPa)	14.08	14.66	14.65	14.68	14.70	14.12	14.65

Table 5: Smart evaluation classification results.

	Date	Classification
1	7.10	Class I
2	7.11	Class II
3	7.12	Class I
4	7.13	Class II
5	7.14	Class III
6	7.15	Class III
7	7.16	Class III

10th and 12th are the first type of sampling. On the 11th and 13th, the classification results of the sampling were the second category of sampling. The classification results of the extraction on the 14th, 15th, and 16th were the extraction category III. The verification shows that the CNN drainage intelligent evaluation model is used to effectively evaluate the gob pressure relief gas drainage.

5. Conclusions

Pressure relief mining combined with gas drainage is an effective method to achieve safe and efficient mining of high gas carbon coal seams. The key problem in evaluating the effect of pressure relief gas drainage in goaf is the accurate construction of the drainage evaluation model. Effective selection of gas drainage evaluation indicators and training of a large number of historical data for evaluation indicators can further improve the accuracy of the gas drainage evaluation model for pressure relief in goaves.

Data Availability

The datasets generated during and/or analyzed during the current study are not publicly available due to sensitivity and data use agreement.

Conflicts of Interest

The author declares that there are no conflicts of interest.

References

[1] J. Zhang, Y. Liu, P. Ren, H. Han, and S. Zhang, "A fully multifield coupling model of gas extraction and air leakage for in-seam borehole," *Energy Reports*, vol. 7, no. 3, pp. 1293–1305, 2021.

[2] A. R. Evanoski-Cole, K. A. Gebhart, B. C. Sive et al., "Composition and sources of winter haze in the Bakken oil and gas extraction region," *Atmospheric Environment*, vol. 156, no. MAY, pp. 77–87, 2017.

[3] A. Goodman, S. Sanguinito, M. Tkach et al., "Investigating the role of water on CO 2 -Utica Shale interactions for carbon storage and shale gas extraction activities – evidence for pore scale alterations," *Fuel*, vol. 242, no. APR.15, pp. 744–755, 2019.

[4] X. Zhao, D. Luo, K. Lu, X. Wang, and C. Dahl, "How the removal of producer subsidies influences oil and gas extraction: a case study in the Gulf of Mexico," *Energy*, vol. 166, no. JAN.1, pp. 1000–1012, 2019.

[5] J. Andersson-Hudson, J. Rose, M. Humphrey, W. Knight, and S. O'Hara, "The structure of attitudes towards shale gas extraction in the United Kingdom," *Energy Policy*, vol. 129, no. JUN, pp. 693–697, 2019.

[6] C. Perera, C. H. Liu, and S. Jayawardena, "The emerging internet of things marketplace from an industrial perspective: a survey," *IEEE Transactions on Emerging Topics in Computing*, vol. 3, no. 4, pp. 585–598, 2015.

[7] B. L. R. Stojkoska and K. V. Trivodaliev, "A review of Internet of Things for smart home: challenges and solutions," *Journal of Cleaner Production*, vol. 140, no. 3, pp. 1454–1464, 2017.

[8] J. Ni, K. Zhang, X. Lin, and X. S. Shen, "Securing fog computing for internet of things applications: challenges and solutions," *IEEE Communications Surveys & Tutorials*, vol. 20, no. 1, pp. 601–628, 2018.

[9] H. Li, K. Ota, and M. Dong, "Learning IoT in edge: deep learning for the internet of things with edge computing," *IEEE Network*, vol. 32, no. 1, pp. 96–101, 2018.

[10] E. Siow, T. Tiropanis, and W. Hall, "Analytics for the internet of things: a survey," *ACM Computing Surveys*, vol. 51, no. 4, pp. 1–36, 2019.

[11] W. Yu, F. Liang, X. He et al., "A survey on the edge computing for the internet of things," *IEEE Access*, vol. 6, no. 99, pp. 6900–6919, 2018.

[12] T. You and S. Balamurugan, "Internet of things-assisted integrated framework for electronic market application," *The Electronic Library*, vol. 40, no. 1/2, pp. 1–17, 2022.

[13] L. Guo, Z. Li, W. C. Yau, and S. Y. Tan, "A decryptable Attribute-based keyword search scheme on eHealth cloud in internet of things platforms," *IEEE Access*, vol. 8, no. 99, pp. 26107–26118, 2020.

[14] M. Helu, T. Sprock, D. Hartenstine, R. Venketesh, and W. Sobel, "Scalable data pipeline architecture to support the industrial internet of things," *CIRP Annals*, vol. 69, no. 1, pp. 385–388, 2020.

[15] S. E. Collier, "The emerging enernet: convergence of the smart grid with the internet of things," *IEEE Industry Applications Magazine*, vol. 23, no. 2, pp. 12–16, 2017.
[16] A. Mosenia and N. K. Jha, "A comprehensive study of security of internet-of-things," *IEEE Transactions on Emerging Topics in Computing*, vol. 5, no. 4, pp. 586–602, 2017.
[17] J. H. Pikul and H. Ning, "Powering the internet of things," *Joule*, vol. 2, no. 6, pp. 1036–1038, 2018.
[18] S. Esterhuyse, M. Avenant, N. Redelinghuys et al., "Monitoring of unconventional oil and gas extraction and its policy implications: a case study from South Africa," *Energy Policy*, vol. 118, no. JUL, pp. 109–120, 2018.
[19] M. Dumiak, "Gas extraction, earthquakes prompt Dutch introspection," *Engineering News-Record*, vol. 280, no. 11, p. 18, 2018.
[20] K. Saito, "Oil pollution and poisoning of the wild bird in hokkaido, and the threat of the "sakhalin oil and gas extraction projects"," *Japanese Journal of Zoo and Wildlife Medicine*, vol. 22, no. 4, pp. 73–78, 2017.